ORCA – Online Research @ Cardiff

Cauchy-Rician Model for Backscattering in Urban SAR Images

Oktay Karakuş, Ercan E. Kuruoğlu, Alin Achim, Mustafa A. Altınkaya,

Abstract

This paper presents a new statistical model for urban scene SAR images by combining the Cauchy distribution, which is heavy tailed, with the Rician back-scattering. The literature spans various well-known models most of which are derived under the assumption that the scene consists of multitudes of random reflectors. This idea specifically fails for urban scenes since they accommodate a heterogeneous collection of strong scatterers such as buildings, cars, wall corners. Moreover, when it comes to analysing their statistical behaviour, due to these strong reflectors, urban scenes include a high number of high amplitude samples, which implies that urban scenes are mostly heavy-tailed. The proposed Cauchy-Rician model contributes to the literature by leveraging non-zero location (Rician) heavy-tailed (Cauchy) signal components. In the experimental analysis, the Cauchy-Rician model is investigated in comparison to state-of-the-art statistical models that include $\mathcal{G}_0$, generalized gamma, and the lognormal distribution. The numerical analysis demonstrates the superior performance and flexibility of the proposed distribution for modelling urban scenes.

Index Terms

Urban modelling, SAR Imaging, Cauchy-Rician distribution.

I. Introduction

THE statistical distribution of a synthetic aperture radar (SAR) signal, that is received via a coherent summation of many elementary echoes [1], is related to the spatial resolution, the wavelength of the sensor, and the size of targets in the scene, which thus makes this problem scale-dependent. Specifically for the homogeneous regions, having low-or-high resolution pixels can be easily neglected since the targets in a homogeneous scene have similar statistical characteristics. However, speaking of heterogeneous regions (especially high-resolution ones), these scenes will be highly complex for modelling issues since they will include various different targets with different statistical characteristics such as buildings, grasslands, sea surface, etc. It is widely known in the literature that some distributions that are considered to be robust for modeling homogeneous regions fail to model high-resolution heterogeneous regions. Regarding the SAR sensor wavelength, since each of those creates different surface penetrations, their corresponding radar return will surely be different, and hence their statistical characteristics. The literature abounds with numerous statistical models, which are either based on the physics of the imaging process or empirical, and all these models have advantages and disadvantages according to the scene type, spatial resolutions and/or frequency band employed.

This paper concerns deriving a candidate statistical model with just two parameters for highly heterogeneous SAR scenes and competing with the state-of-the-art. Particularly, we focus on the statistical modelling of urban areas in SAR imagery, which are characterised by a high number of strong scatterers caused by man-made structures with dihedral or trihedral configurations [2].

The standard model for the back-scattered SAR signal from a given area corresponds to a complex signal, generically expressed as $R = x_1 + jx_2$ [3], [4]. The simplest model for SAR amplitude assumes the real (x_1) and imaginary (x_2) parts are independent and identically distributed (i.i.d.) zero-mean Gaussian random variables. This
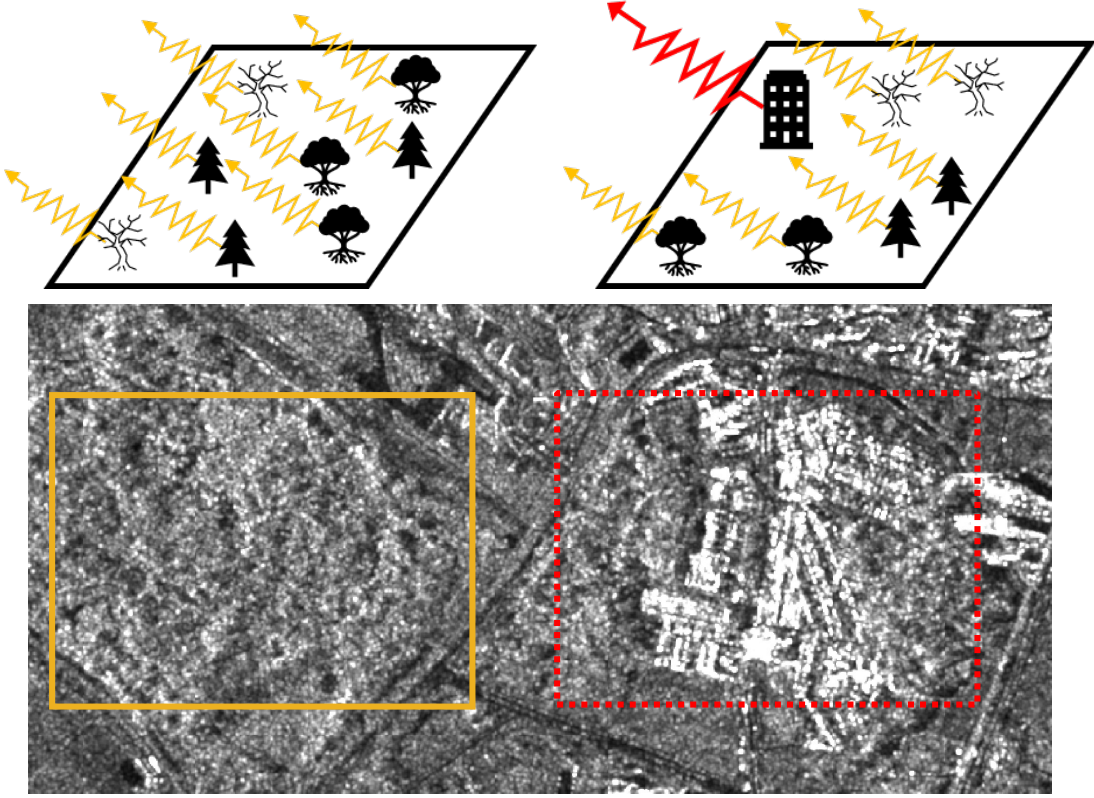
Fig. 1. Surface scattering examples. (left): distributed scattering. (right): a number of strong scatterers.

determines a Rayleigh model for the SAR distribution of the amplitude $r = \sqrt{x_1^2 + x_2^2}$, which is valid provided there are no dominating scatterers in the scene. When this assumption is violated, the real and imaginary signal components become non-zero mean ($\delta \neq 0$) Gaussian, which then determines a Rician distribution for SAR images in amplitude format. The Rician model is widely used to characterise SAR scenes containing many strong back-scattered echoes. These include natural targets such as forest canopy, mountain tops, sea waves, as well as some man-made structures with dihedral or trihedral configurations such as cars, buildings, or vessels [2], [5]–[8].

Notwithstanding their appealing theoretical properties and simple analytical structure, statistical models based on the Gaussian assumption (Rayleigh-Rician) do not reflect real life phenomena such as those encountered when SAR reflections exhibit impulsive behaviour indicative of underlying heavy-tailed distributions. Thus, numerous statistical models in the literature were developed to account for non-Rayleigh cases, and proved to be effective for modeling SAR imagery. A non-exhaustive list of models include Gamma [9], [10], Weibull [11], [12], lognormal [13], $\mathcal{K}$ [9], [14], $\mathcal{G}_0$ [10], [15], [16], generalized gamma (GΓD) [17], [18], stable-Rayleigh [3], [19], and generalised-Gaussian Rayleigh [4]. Incorporating into the Rician model the non-Gaussian and heavy-tailed characteristics of SAR signals through a Laplace distribution, as in [20], [21], addresses many of the limitations of the above models. The resulting Laplace-Rician model is based on the assumption that back-scattered SAR signal components are Laplace distributed and was shown to achieve superior performance in modeling amplitude SAR images corresponding to various types of scenes, such as sea surface, [20], forest, or agricultural [21].

In recent work [22], we have extended the Laplace-Rician model by proposing a much more general framework, whereby the back-scattered SAR signal components are *non-zero mean Generalized-Gaussian* (GG) distributed. We have demonstrated the flexibility and accuracy of the GG-Rician model in modelling both amplitude and intensity SAR images corresponding to a variety of contents, including urban scenes, agricultural, land cover, and the sea surface.

Despite the success of the GG-Rician and Laplace-Rician distributions, we observed that GG-Rician's modelling performance can sometimes be lower than the GΓD and $\mathcal{G}_0$ models. Such is the case for urban SAR scenes, which include a high number of strong scatterers. We attribute this to the fact that the heavy-tailed characteristics of most

of the generalized Gaussian family densities (e.g. Laplace, and the ones with $\alpha > 1$) might not be impulsive enough to faithfully capture the characteristics of scenes with a high number of large intensity values. Consequently, in this paper, we propose the use of the Cauchy distribution for modelling the backscattered SAR signal real and imaginary components in urban images whilst keeping the Rician base model via non-zero location parameter of the Cauchy density.

II. THEORETICAL BACKGROUND

A. On the Rician Assumption

As was mentioned in the previous section, the fundamental Rayleigh backscattering idea relies on the assumption that the scene does not have any dominating scatterer whilst having a distributed scattering mechanism. However, in various scenes such as urban ones, the illuminated area may include one (or a small number of) dominating scatterer(s) (Fig. 1 - (upper right)), and a large number of non-dominant ones [23]. This phenomenon can also be seen in a real SAR image in Fig. 1. The displayed scene within the rectangle on the left is a good example of the distributed scattering, whilst radar returns in the rectangle on the right include various urban scene targets (buildings, wall corners, etc.). Therefore, the scene on the right includes quite a lot of high intensity returns, resulting in non-distributed scattering. Hence, the assumption on which the Rayleigh backscattering model is based upon would no longer be valid. From a statistical point of view, this corresponds to a situation whereby the signal components x and y are still i.i.d. random variables, but with non-zero-means. When the signal components are Gaussian, this determines Rician backscattering.

To motivate the Rician assumption employed in this letter, two different patches (urban and sea surface) from a SAR scene were investigated. The COSMO-SkyMed SAR data used for this purpose includes an intensity SAR scene as well as in-phase ($\mathcal{I}$) and quadrature ($\mathcal{Q}$) components of the back-scattered SAR signal. For both urban and sea patches, histograms of $\mathcal{I}$ and $\mathcal{Q}$ components were calculated and they are depicted in Fig. 2. It is clear from Fig. 2 that sea and urban scenes have characteristically different component distributions. Sea surface components are centred around the origin (potentially Rayleigh based) with a mostly symmetric form whilst distributions for urban components are skewed and centred around a "non-zero" data value. This simple example provides a physical support to the use of Rician backscattering specifically for urban SAR scenes.

B. On the Choice of Cauchy Distribution

The Cauchy distribution is known to be heavy-tailed and to promote (statistical) sparsity in various applications. From a purely theoretical viewpoint, our preference for the Cauchy model over other candidate models stems from its membership of the α-Stable family of distributions. Specifically, unlike other empirical distributions able to faithfully fit distributions with heavy-tails, α-stable distributions are motivated by the generalised central limit theorem (CLT) similarly to the way Gaussian distributions are motivated by the classical CLT. Contrary to the general α-stable family, the Cauchy distribution has a closed-form probability density function, with dispersion (scale) parameter γ, which controls the spread of the distribution, and the location parameter δ.

Despite the remarkable performance of the Laplace-Rician model [20], [21] in modelling various types of SAR scenes, our motivation is to provide an amplitude model for urban SAR scenes, which clearly show heavy-tailed characteristics, since they have more pronounced single reflectors when compared to, for example, sea surface images. In the mini-figure of Fig. 2, we compare tail behaviours of Laplace and Cauchy distributions for equal location parameters. It is clear from this visual representation that the Cauchy model has more mass in the tails indicating better potential for modelling impulsive characteristics. It is also interesting to note that the differences between Laplace and Cauchy pdfs in terms of tails depicted in the mini figure in Fig. 2 resemble the differences between sea and urban scenes in Fig. 2. To this end, Fig. 2 also provides support to the need for heavier tailed density for the urban scene modelling.

III. THE CAUCHY-RICIAN DENSITY

We first start by assuming that the signal components, x_1 and x_2 are non-zero Cauchy distributed as $x_1 \sim \mathcal{Ca}(\delta, \gamma)$ and $x_2 \sim \mathcal{Ca}(\delta, \gamma)$. Consider the bivariate isotropic Cauchy distribution, whose characteristic function has the form
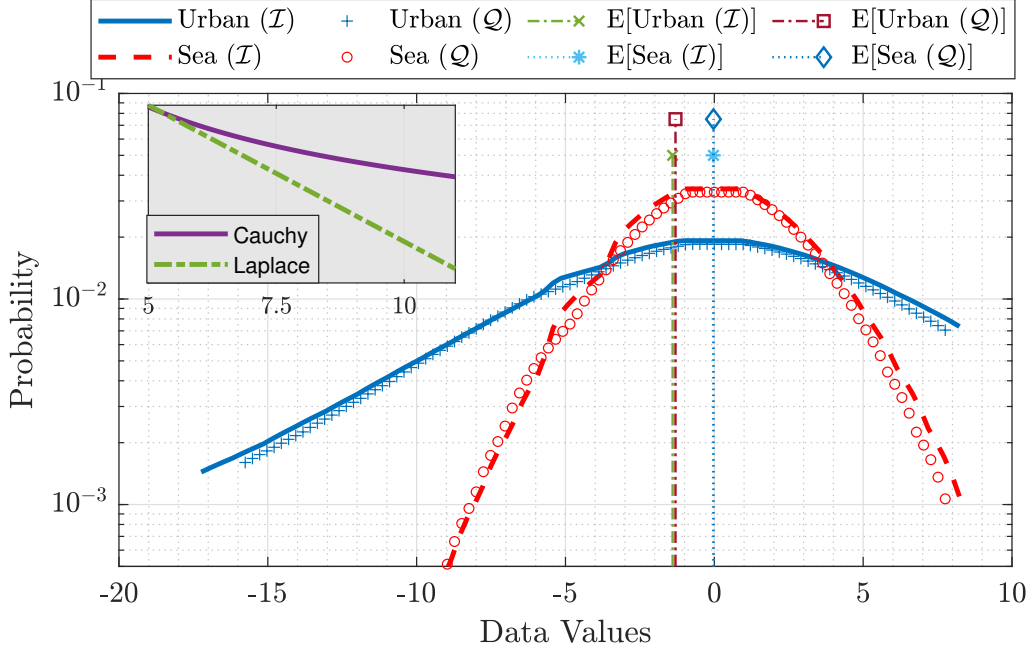
Fig. 2. Comparison for $\mathcal{I}$ and $\mathcal{Q}$ components of different SAR scenes. Mini-figure with darker background: Laplace pdf *vs.* Cauchy pdf.

of $\psi(t_1, t_2) = \exp(j\delta(t_1 + t_2) - \gamma|\mathbf{t}|)$, where t_1 and t_2 are components of the vector $\mathbf{t}$, and $|\mathbf{t}|$ is the magnitude. The probability density function (pdf) can be evaluated by taking the 2D Fourier transform as

$$f(x_1, x_2) = \frac{1}{(2\pi)^2} \int_{t_1} \int_{t_2} \exp(j\delta(t_1 + t_2)) \exp(-\gamma|\mathbf{t}|) \exp(-j(x_1 t_1 + x_2 t_2)) dt_1 dt_2. \tag{1}$$

We make a change of variables and rewrite x_1 and x_2 in terms of variables y_1 and y_2, respectively as $y_1 = x_1 - \delta$, and $y_2 = x_2 - \delta$, which leads to

$$f(y_1 + \delta, y_2 + \delta) = \frac{1}{(2\pi)^2} \int_{t_1} \int_{t_2} \exp(-\gamma|\mathbf{t}|) \exp\{-j[t_1 y_1 + t_2 y_2]\} dt_1 dt_2. \tag{2}$$

We now convert this integral into the polar coordinates via $t_1 = u\cos\phi$ and $t_2 = u\sin\phi$

$$f(y_1 + \delta_1, y_2 + \delta_2) = \int_0^{2\pi} \int_0^\infty \frac{u\exp(-\gamma u)}{(2\pi)^2} \exp\{-ju[y_1\cos\phi + y_2\sin\phi]\} du d\phi. \tag{3}$$

where $u = |\mathbf{t}|$ and $\phi = \arctan(t_1/t_2)$. If we reorganise (3), we further obtain

$$f(y_1 + \delta_1, y_2 + \delta_2) = \frac{1}{2\pi} \int_0^\infty u\exp(-\gamma u) \left[\frac{1}{2\pi} \int_0^{2\pi} \exp\left(-ju[y_1\cos\phi + y_2\sin\phi]\right) d\phi \right] du. \tag{4}$$

From [24], the expression in square brackets becomes $\mathcal{J}_0(u|\mathbf{y}|)$, where $\mathcal{J}_0$ is the zeroth order Bessel function of the first kind. We then rewrite (4) as [3]

$$f(y_1 + \delta_1, y_2 + \delta_2) = \frac{1}{2\pi} \int_0^\infty u\exp(-\gamma u^\alpha) \mathcal{J}_0(u|\mathbf{y}|) du. \tag{5}$$

We now have a bivariate density, and to derive the density function in amplitude form, we take the following polar transformation

$$f(r, \theta) = rf(y_1 + \delta = r\cos\theta, y_2 + \delta = r\sin\theta), \tag{6}$$

where $r \geq 0$ and $0 \leq \theta \leq 2\pi$. Then, marginalising over θ leads to

$$f(r) = \frac{r}{2\pi} \int_0^{2\pi} \int_0^\infty u\exp(-\gamma u) \mathcal{J}_0(uA(r, \theta)) du d\theta. \tag{7}$$

where $A(r, \theta) = \sqrt{r^2 + 2\delta^2 - 2r\delta(\cos\theta + \sin\theta)}$. Reorganising (7), we have

$$f(r) = \frac{r}{2\pi} \int_0^{2\pi} d\theta \int_0^\infty u \exp(-\gamma u)\mathcal{J}_0(uA(r,\theta))du. \tag{8}$$

Using the identity below [25]

$$\int_0^\infty z^{n+1} \exp(-az)\mathcal{J}_n(bz)dz = \frac{a2^{n+1}b^n\Gamma(n+3/2)}{\sqrt{\pi}(a^2 + b^2)^{n+3/2}} \tag{9}$$

where $a > 0$, $b > 0$ and $n > -1$, we rewrite (8) for $n = 0$ as

$$f(r) = \frac{r\gamma}{2\pi} \int_0^{2\pi} \frac{d\theta}{[\gamma^2 + r^2 + 2\delta^2 - 2r\delta(\cos\theta + \sin\theta)]^{3/2}} \tag{10}$$

which corresponds to the *Cauchy-Rician* distribution. For $\delta = 0$, it is straightforward to show that the distribution in (10) reduces to *Cauchy-Rayleigh* distribution from [3] as $f(r) = r\gamma/(r^2 + \gamma^2)^{3/2}$. The Cauchy-Rician distribution has the capability to model multi-look SAR imagery and also has a form for modelling intensity SAR images. However, due to page limitations, we thus leave presenting these capabilities of the proposed model as future work.

Since the pdf expression in (10) is not in a compact analytical form and it does not seem to be possible to invert it to obtain parameter values, we employ a Bayesian sampling methodology in order to estimate model parameters of γ and δ. For this reason, in this paper, we adjusted the method presented in [20], for the Cauchy-Rician density parameter estimation by simply replacing the likelihood densities from Laplace-Rician to Cauchy-Rician. In particular, the method is a Metropolis-Hastings (MH) algorithm, and in each iteration, it applies one of 3 different moves: $\mathcal{M}_1$: Update δ for fixed γ, $\mathcal{M}_2$: Update γ for fixed δ, $\mathcal{M}_3$: Update γ and δ where the probabilities of which are selected as 0.4, 0.4 and 0.2 for $\mathcal{M}_1$, $\mathcal{M}_2$ and $\mathcal{M}_3$, respectively.

IV. EXPERIMENTAL RESULTS

To test the proposed parameter estimation method, we created 100 simulated Cauchy-Rician sequences (1500 samples for each) for randomly selected parameters in intervals of $\delta \to (0, 50]$ and $\gamma \to (0, 20]$. For each simulated data set, the parameter estimation method was used to estimate δ and γ, and the results are presented in Figure 3. Evaluating the boxplot in Figure 3-(a), we can state that the parameter estimation method shows remarkable performance as e.g. *Kullback-Leibler* (KL) divergence values are relatively small (less than 0.1) whilst Kolmogorov-Smirnov (KS) p-values are greater than 0.9999 for all data sets. Evaluating the boxplot in Figure 3-(a) for the first four boxes, the parameter estimation values show that the location parameter δ estimates are generally close to the real values whilst overestimation can sometimes be observed for the scale parameter γ estimation results. This overestimation might cause by the number of samples utilised in this first simulation case. Increasing the number of samples, we believe, might reduce γ estimation results. In Figure 3-(b), we show that the estimation performance of the method is independent of the initial values of δ and γ, where the MCMC based approach reaches the correct values via a random walk by performing an accept/reject based sampling.

The proposed statistical model was tested on various urban SAR data. We subsequently conducted experiments to determine the best fitting distribution for a given real urban SAR images. Since each goodness of fit method to be utilised to measure modeling performance can have various advantages or disadvantages due to such as sample size, estimated parameters, spatial resolution, in order to compensate for this, we used (1) KL divergence, (2) residual standard error (RSE), (3) the corrected Akaike information criterion (AICc) [26], (4) Anderson-Darling (AD) test [27], (5) KS p-value and (6) the log-likelihood (logLHD). The proposed method was tested on 20 different urban SAR images coming from TerraSAR-X, COSMO-SkyMed and ICEYE. The performance of the Cauchy-Rician model was compared to Laplace-Rician, Lognormal, $\mathcal{G}_0$, and GΓD distributions. It is worth noting that other common models such as the Rayleigh, Gamma, and $\mathcal{K}$ distributions have been left aside from our simulations, since our previous work has shown that they are less successful than the utilised reference models [22]. The results are depicted in Figures 4 and 5.

On evaluating the sub-figures in Fig. 4-(a)-(c), the superiority of the proposed method can been seen from the RSE, p-value heatmaps. The Cauchy-Rician model is the best model for all urban SAR scenes in terms of the RSE and AICc values, whilst p-values are mostly distributed between Cauchy-Rician, $\mathcal{G}_0$ and Lognormal models. In terms of the KL divergence results in Fig. 4-(d) for overall percentages, we can see that even though the proposed
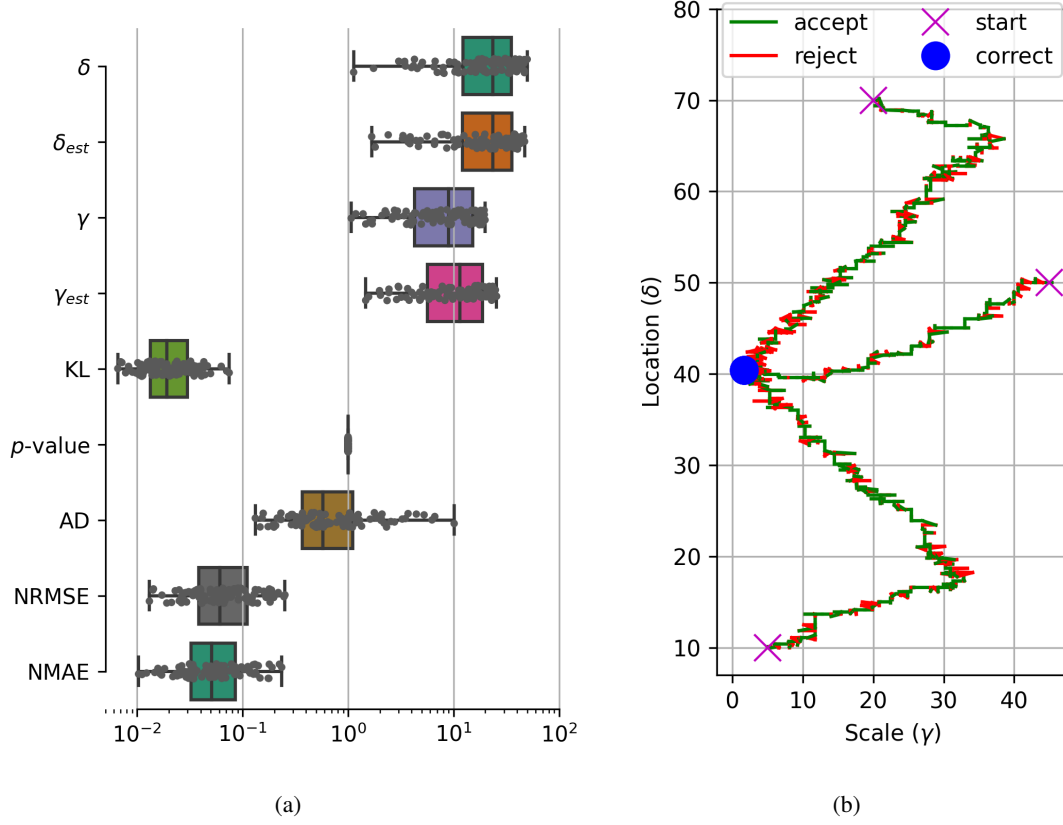
Fig. 3. MCMC-based parameter estimation results. (a) Performance metrics. (b) Random-walks for three different initial $[\delta, \gamma]$ pairs.

model is the best model for 35% of the total 20 SAR scenes, $\mathcal{G}_0$ and Laplace-Rician models also perform well in terms of AD test scores.

Fig. 5 presents SAR image of an example urban scene and is modeling results in logarithmic scale. The log-scale pdf modeling results in Fig. 5 (b)-(left) confirm the numerical results presented in Fig. 4. Despite resulting in slight overestimation around the peak of the histogram, the Cauchy-Rician outperforms most of the reference models utilised in this study due to its accuracy in modelling the tails of the distribution.

In order to quantitatively evaluate the tail modelling performance of the Cauchy-Rician model, we also performed a simulation experiment for only the tails of the image histograms for $CDF(I_i) \geq 0.75$ and $CDF(I_i) \geq 0.90$. In order to measure how accurate the tail modelling is, we used negative log-likelihood ratio ($-\log$LHD) and decided the best model which minimises the $-\log$LHD. Fig. 4-(d) presents the percentages of SAR scenes for two different experiments. It can be seen from the barplots that the proposed Cauchy-Rician density achieves better tail modelling compared to state-of-the-art models such as $\mathcal{G}_0$, and GΓD despite having only two model parameters. Fig. 5 (b)-(right) also provides a visual demonstration of the tail modelling performance.

V. Conclusion

This paper introduced the Cauchy-Rician distribution to characterise the amplitude of the complex back-scattered SAR signal from urban scenes. Following the theoretical and physical aspects of the urban SAR scenes, the proposed approach leverages both heavy-tailed distributions and the Rician back-scattering. Thanks to Cauchy distribution's ability to model heavy-tails, the proposed model further extends the idea behind GG-Rician density [22] for SAR scenes that require heavier tails than that of GG-Rician. Despite having only two model parameters and exploiting only one member of α-Stable distributions, the Cauchy-Rician density demonstrates considerable improvement in performance compared to the state-of-the-art advanced models such as $\mathcal{G}_0$ and GΓD.

References

[1] E. Dalsasso, L. Denis, and F. Tupin, "As if by magic: self-supervised training of deep despeckling networks with MERLIN," *IEEE Transactions on Geoscience and Remote Sensing*, pp. 1–1, 2021.
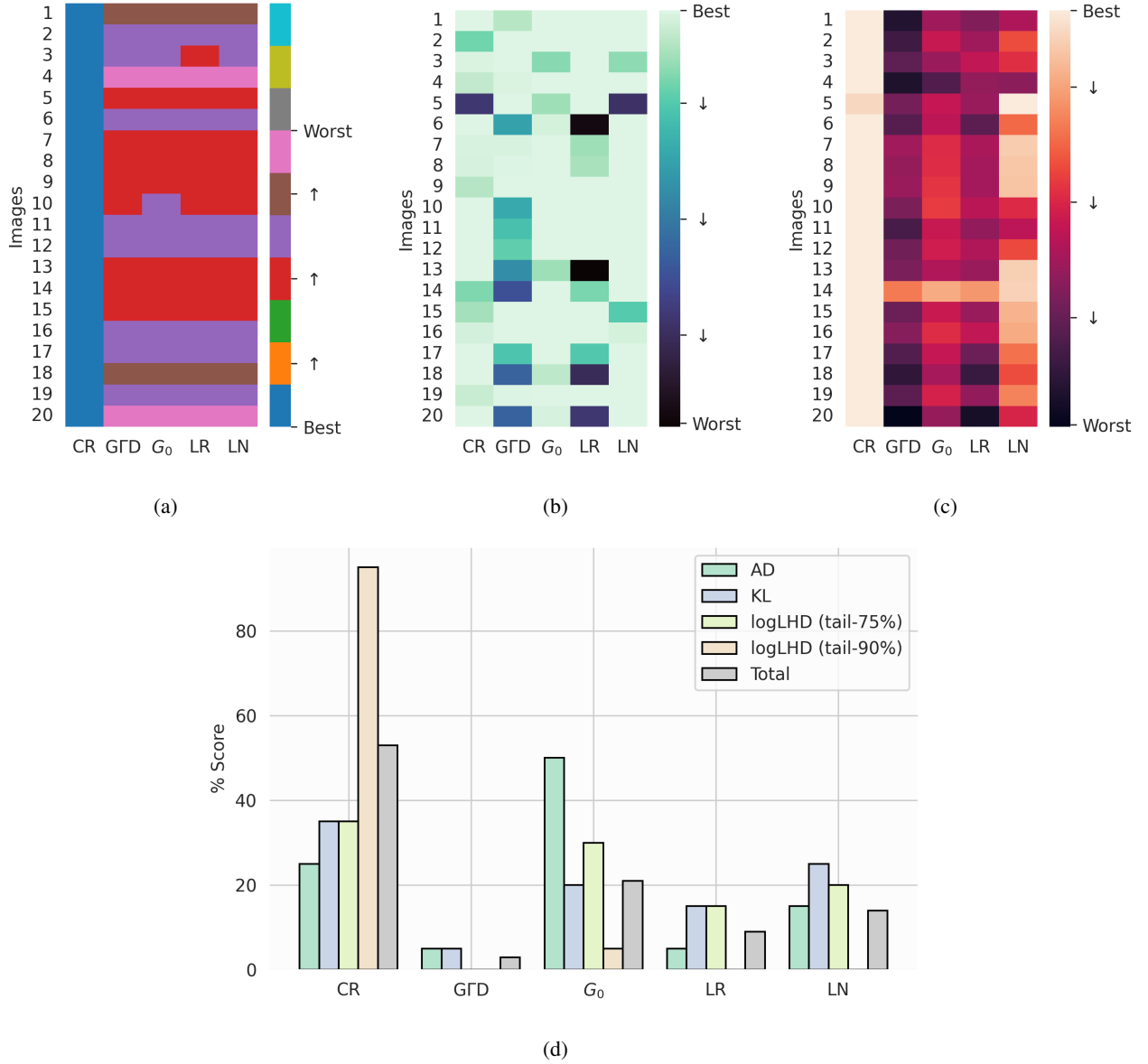
Fig. 4. Modeling performance analysis. Heatmap representations of (a) RSE, (b) KS *p*-values, and (c) AICc. (d) Percentages of being the best model among 20 images in terms of the measures of KL, AD, LogLHD and Total. To calculate the Total % Score, all statistical models are assessed in terms of RSE, AICc, KL, AD, and *p*-value measures. For each measure, percentages of being the best model are calculated and combined to obtain Total % Score (E.g. 50% means being the best models in terms of the half of the error measures). CR: Cauchy-Rician, LR: Laplace-Rician, LN: Lognormal.

[2] J. M. Nicolas and F. Tupin, "A new parameterization for the Rician distribution," *IEEE Geoscience and Remote Sensing Letters*, vol. 17, no. 11, pp. 2011–2015, 2020.

[3] E. E. Kuruoglu and J. Zerubia, "Modeling SAR images with a generalization of the Rayleigh distribution," *IEEE Transactions on Image Processing*, vol. 13, no. 4, pp. 527–533, 2004.

[4] G. Moser, J. Zerubia, and S. B. Serpico, "SAR amplitude probability density function estimation based on a generalized Gaussian model," *IEEE Transactions on Image Processing*, vol. 15, no. 6, pp. 1429–1442, 2006.

[5] J. W. Goodman, "Statistical properties of laser speckle patterns," in *Laser speckle and related phenomena*. Springer, 1975, pp. 9–75.

[6] T. Eltoft, "The Rician inverse Gaussian distribution: a new model for non-Rayleigh signal amplitude statistics," *IEEE Transactions on Image Processing*, vol. 14, no. 11, pp. 1722–1735, 2005.

[7] G. Gao, "Statistical modeling of SAR images: A survey," *Sensors*, vol. 10, no. 1, pp. 775–795, 2010.

[8] W. Wu, H. Guo, and X. Li, "Man-made target detection in urban areas based on a new azimuth stationarity extraction method," *IEEE Journal of Selected Topics in Applied Earth Observations and Remote Sensing*, vol. 6, no. 3, pp. 1138–1146, 2013.

[9] J. Sun, X. Wang, X. Yuan, Q. Zhang, C. Guan, and A. V. Babanin, "The Dependence of Sea SAR Image Distribution Parameters on Surface Wave Characteristics," *Remote Sensing*, vol. 10, no. 11, p. 1843, 2018.
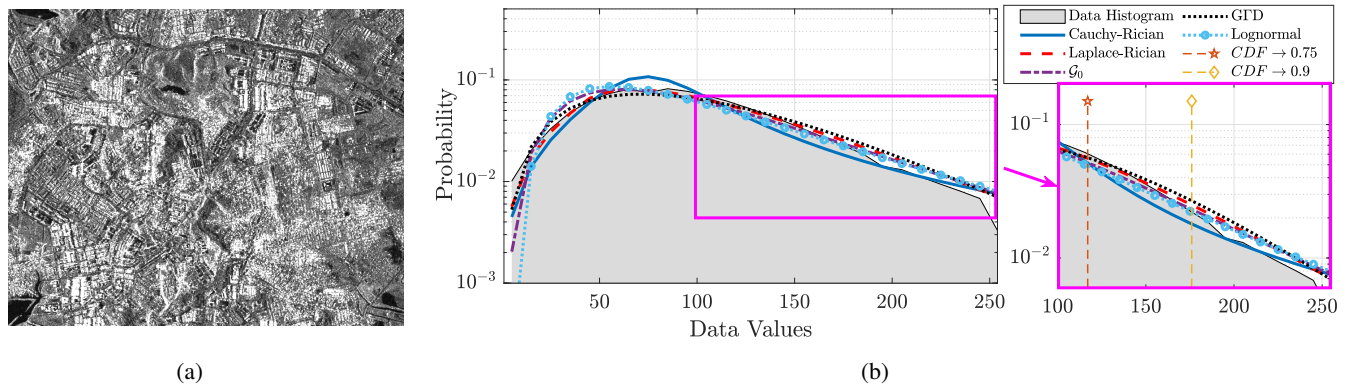
(a)

(b)

Fig. 5. Visual evaluation of SAR amplitude models. (a) Urban SAR Scene. (b)-(left) Log-pdf of SAR image in (a) and model fits. (b)-(right) The zoomed-in axis for the tail of the histogram with model fits.

[10] S. Cui, G. Schwarz, and M. Datcu, "A comparative study of statistical models for multilook SAR images," *IEEE Geoscience and Remote Sensing Letters*, vol. 11, no. 10, pp. 1752–1756, 2014.

[11] S. Chitroub, A. Houacine, and B. Sansal, "Statistical characterisation and modelling of SAR images," *Signal Processing*, vol. 82, no. 1, pp. 69–92, 2002.

[12] J. R. M. Fernández, "Estimation of the relation between Weibull sea clutter and the CA-CFAR scale factor," *Revista Ingeniería*, vol. 25, no. 2, pp. 19–28, 2015.

[13] Z. Chen, X. Liu, Z. Wu, and X. Wang, "The Analysis of Sea Clutter Statistics Characteristics Based on the Observed Sea Clutter of Ku-Band Radar," in *2013 Proceedings of the International Symposium on Antennas & Propagation*, vol. 2. IEEE, 2013, pp. 1183–1186.

[14] M. Migliaccio, L. Huang, and A. Buono, "SAR speckle dependence on ocean surface wind field," *IEEE Transactions on Geoscience and Remote Sensing*, vol. 57, no. 8, pp. 5447–5455, 2019.

[15] A. C. Frery, H.-J. Muller, C. d. C. F. Yanasse, and S. J. S. Sant'Anna, "A model for extremely heterogeneous clutter," *IEEE transactions on geoscience and remote sensing*, vol. 35, no. 3, pp. 648–659, 1997.

[16] S. Cui and M. Datcu, "Coarse to fine patches-based multitemporal analysis of very high resolution satellite images," in *2011 6th International Workshop on the Analysis of Multi-Temporal Remote Sensing Images (Multi-Temp)*. IEEE, 2011, pp. 85–88.

[17] E. W. Stacy *et al.*, "A generalization of the gamma distribution," *The Annals of mathematical statistics*, vol. 33, no. 3, pp. 1187–1192, 1962.

[18] H.-C. Li, W. Hong, Y.-R. Wu, and P.-Z. Fan, "On the empirical-statistical modeling of SAR images with generalized gamma distribution," *IEEE Journal of selected topics in signal processing*, vol. 5, no. 3, pp. 386–397, 2011.

[19] O. Karakuş, E. E. Kuruoğlu, and M. A. Altınkaya, "Generalized Bayesian model selection for speckle on remote sensing images," *IEEE Transactions on Image Processing*, vol. 28, no. 4, pp. 1748–1758, 2018.

[20] O. Karakuş, E. E. Kuruoglu, and A. Achim, "Modelling sea clutter in SAR images using Laplace-Rician distribution," in *ICASSP 2020 - 2020 IEEE International Conference on Acoustics, Speech and Signal Processing (ICASSP)*, 2020, pp. 1454–1458.

[21] O. Karakus, E. E. Kuruoglu, and A. Achim, "A Modification of Rician Distribution for SAR Image Modelling," in *EUSAR 2021; 13th European Conference on Synthetic Aperture Radar*. VDE, 2021, pp. 1–6.

[22] O. Karakuş, E. E. Kuruoğlu, and A. Achim, "A generalized Gaussian extension to the Rician distribution for SAR image modeling," *IEEE Transactions on Geoscience and Remote Sensing*, 2021.

[23] D. Yue, F. Xu, A. C. Frery, and Y. Jin, "SAR image statistical modeling : Part one–single-pixel statistical models," *IEEE Geoscience and Remote Sensing Magazine*, pp. 0–0, 2020.

[24] M. Abramowitz and I. A. Stegun, *Handbook of mathematical functions: with formulas, graphs, and mathematical tables*. Courier Corporation, 1965, vol. 55.

[25] I. S. Gradshteyn and I. M. Ryzhik, *Table of integrals, series, and products*. Academic press, 2014.

[26] J. E. Cavanaugh and A. A. Neath, "The Akaike information criterion: Background, derivation, properties, application, interpretation, and refinements," *Wiley Interdisciplinary Reviews: Computational Statistics*, vol. 11, no. 3, p. e1460, 2019.

[27] F. W. Scholz and M. A. Stephens, "K-sample Anderson–Darling tests," *Journal of the American Statistical Association*, vol. 82, no. 399, pp. 918–924, 1987.